Ablative Z-Pinch Pulsed Plasma Thruster

T.E. Markusic[*], K.A. Polzin[†], J.Z. Levine[‡], C.A. McLeavey[§], and E.Y. Choueiri[¶]
Electric Propulsion and Plasma Dynamics Laboratory (EPPDyL)
Mechanical and Aerospace Engineering Department
Princeton University, Princeton, New Jersey 08544

AIAA 2000-3257[‖]

July 17, 2000

Abstract

The Z-pinch configuration in gas-fed devices was adapted for an ablative Pulsed Plasma Thruster (PPT). The motivation stems from the promise of the Z-pinch configuration for increasing the thrust-to-power ratio and mass utilization efficiency. A series of ablative Z-pinch PPTs were constructed and their performance measured using a swinging gate thrust stand and mass ablation measurements. Several iterations of the design lead to the selection of a thruster with an augmented "spike" inner electrode for more exhaustive testing. Peak performance parameters for this configuration were found to be: $I_{sp} = 574$ s, η_t = 7.5 %, and T/P = 28 μN/W. In order to determine whether the plamsa was pinching, photographs of the discharge were acquired using a modified thruster having transparent Plexiglas propellant and mesh sidewalls. A current sheet structure leading to a plasma pinch was observed.

[*]Graduate Student, US Air Force Palace Knight. Member AIAA.

[†]Graduate Student, Member AIAA.

[‡]Undergraduate Student.

[§]Undergraduate Student.

[¶]Chief Scientist at EPPDyL. Assistant Professor, Applied Physics Group. Senior Member AIAA.

[‖]Presented at the 36^{th} AIAA Joint Propulsion Conference, Huntsville, Alabama, July 16-19, 2000.

1 Introduction

There is presently a strong, renewed interest in PPTs for a wide range of space missions, especially ablative PPTs (see, for example Burton and Turchi [1] and Martinez-Sanchez and Pollard [2]). PPTs have the potential of fulfilling the attitude control role on a satellite at greatly reduced mass and cost. They are also being considered for constellation maintenance for such missions as interferometric imaging of the Earth from space or deep space from an Earth orbit. The benefits of PPTs are their very small impulse bits ($\sim 10^{-4}$ N-s) for precise satellite motion, reliability, high specific impulse. The ablative version of the PPT uses a solid propellant, such as Teflon, to provide further advantages such as compactness and overall ease of system integration.

Even though there are many missions where PPTs are advantageous with existing performance, the range of applications is expected to greatly increase if their overall performance can be improved – in particular, increased thrust-to-power ratio and thrust efficiency. There are two broad categories of inefficiencies in ablative pulsed plasma thrusters that limit the present thrust efficiency. These include energy inefficiencies which pertain to the efficient transfer of stored capacitor energy into acceleration of the ionized propellant and propellant inefficiencies which include particulate emission and late-time vaporization[3]. In many applications (e.g. high

slew rate maneuvers), higher thrust-to-power ratios are required than can be provided by common versions of the PPT. The main motivation for developing the ablative Z-pinch PPT was to create a thruster with higher thrust-to-power ratios and reasonable efficiencies relative to more common PPT designs by exploitng certain favorable attributes of the Z-pinch geometry.

Until recently, rectangular-geometry PPTs have been the most actively researched ablative PPTs (see, for example,[4, 5, 6]). Burton *et al.*[7] has achieved high thrust-to-power ratios using a side-fed coaxial geometry with a nozzle. Turchi *et al.*[8] has constructed an inverse Z-pinch thruster to test predictions from his analytical optimization models. In the present work, we present a Z-pinch thruster with high thrust-to-power ratio and moderate thrust efficiency compared to commercially available thrusters.

The structure of this paper is as follows. First, the apparatus used in all of the experiments is described. The next section of the report describes the thruster design iteration process. Qualitative references to performance results are made in order to clarify the motivation behind each design modification. The following section presents all the acquired measurements, pointing out important trends and further elucidating the motivation behind the design iteration. The final section summarizes the important findings and suggests future directions. An appendix provides a detailed description of the new test facilities at Princeton's Electric Propulsion and Plasma Dynamics Lab (EPPDyL) and documents the study and control of the level of contamination, which is a crucial issue for unambiguous measurements of low impulse devices.

2 Apparatus

The apparatus used in this experiment consisted of an ablative pulsed plasma thruster mounted on a thrust stand in a large dielectric vacuum facility.

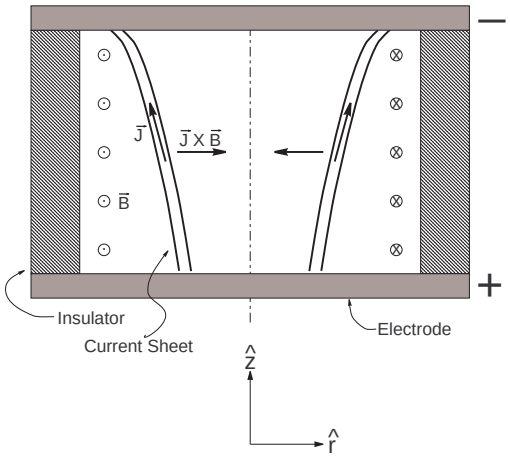

Figure 1: Schematic of the Z-pinch geometry.

2.1 Thruster

The series of thrusters described in this report consists of three Ablative Z-pinch Pulsed Plasma Thrusters, called AZPPT1-3, having a coaxial discharge geometry commonly referred to as linear or Z-pinch. The electrode, arc discharge, and field geometry in a Z-pinch device are shown schematically in figure 1. Z-pinches were originally conceived of as a method for producing hot, dense plasmas for nuclear fusion research. A conventional Z-pinch discharge progresses as follows. First, the volume between two cylindrical disk electrodes, separated by an insulating sidewall, is filled with a working gas. High voltage is then applied between the electrodes (typically a capacitor bank is connected to the electrodes with a high speed switch such as an ignitron.) The gas between the electrodes then breaks down and current begins to flow between the electrodes. The initial current distribution is in the form of a cylindrical current sheet along the face of the insulator. The current sheet forms at the cavity's maximum radius because it is the path of least impedance available to the circuit; in a circuit with rapidly rising current, the inductive voltage drop, $V_L = L\ dI/dt$, dominates the impedance of the system and, hence, the circuit seeks the path of least inductance. As the current rises, an azimuthal magnetic field forms on the out-

side of the current sheet; this magnetic field interacts with the current sheet to create a radially inward directed electromagnetic self-force, $F_{EM} = \vec{J} \times \vec{B}$. This force causes the current sheet to collapse toward the center of the cavity – sweeping up gas along the way. The current sheet does not, however, remain perfectly cylindrical as it progresses toward the center of the cavity. It has been experimentally observed that current sheets tilt, with the anode arc attachment leading the cathode attachment, as the discharge propagates[9]. In particular, this phenomenon is appropriately named the "zipper effect" in Z-pinch devices[10]. When the current sheet reaches the center of the cavity it collapses into a single filament and, provided it has effectively entrained gas during its propagation, produces a compressed column of hot, highly compressed plasma. The filament lifetime is short-lived, as the onset of MHD instabilities rapidly disintegrate the arc.

In the early 60's R.G. Jahn *et al.* showed that the Z-pinch geometry could be modified to create an axially streaming plasma and, hence, a new type of plasma thruster[11]. This was accomplished by simply replacing the solid top electrode (see fig.1) of the conventional Z-pinch geometry with an electrode that had an orifice at its center. It was shown that, after the radial pinching phase, plasma was ejected axially with speeds comparable to the initial pinching phase speeds. The acceleration mechanism in these devices can be explained as follows. The propellant is initially radially accelerated by the imploding current sheet (electromagnetic force). When the sheet is fully pinched, the presence of an orifice in the top electrode results in a large axial pressure gradient (gasdynamic force) and, hence, the plasma accelerates axially out of the thruster. A radial force results in axial motion of the fluid in the absence of an axial constraint as in a toothpaste tube. Evidently, another important consideration in designing a thruster is the effect of polarity which controls the zipper effect. Referring to figure 1, it is apparent that it is desirable to have the the current sheet zip upward, toward the exhaust orifice; otherwise, the current sheet will drive the plasma toward the solid electrode, creating a component of velocity opposite to the desired, thrust producing, direction of flow.

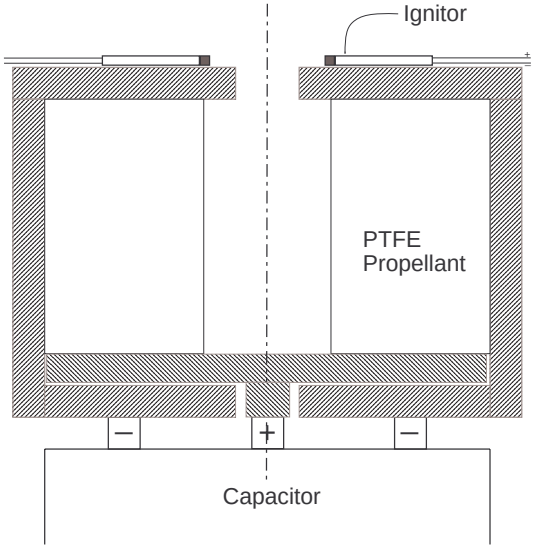

Figure 2: Schematic of the ablative Z-pinch thruster geometry.

2.1.1 Design Motivation

The present development of the AZPPT series began after it was realized that the gas-fed Z-pinch PPT geometry has features which could enhance the performance of ablative PPTs. Potential advantages over existing designs include: mechanical simplicity, structural compactness amenable to miniaturization, lower exhaust beam divergence, higher thrust-to-power ratio, and higher propellant utilization efficiency. These potential benefits will be discussed, in turn, below.

An ablative Z-pinch PPT is structurally very similar to its gas-fed counterpart. The difference is that the sidewalls, aside from providing electrical insulation, also serve as the source of propellant. Figure 2 schematically illustrates the components of an ablative Z-pinch PPT. Operation of the thruster is achieved by charging the capacitor to the desired voltage and then firing the ignitors. In the absence of a gaseous propellant, the ignitors provide enough charge carriers to allow current to start flowing from the main capacitor. The discharge then begins in a manner similar to the gas-fed Z-pinch – a cylin-

drical current sheet rapidly forms at the surface of the polytetrafluoroethylene (PTFE) propellant. The arc ablates PTFE and accelerates it products radially inward. After initiation, the current sheet dynamics for ablative thrusters are not well understood. It is uncertain whether the current sheets collapses radially as in the gas-fed thruster (detonation mode), or if it remains relatively stationary, electromagnetically "blowing" propellant radially inward (deflagration mode). Further, without understanding the current sheet dynamics, it is uncertain how the propellant flow is ultimately "turned" to obtain axial ejection from the cathode orifice. In the design iteration of the AZPPT series it was assumed *a priori* that the current sheet behaves similarly to those observed in gas-fed devices. A later experiment, which is described in section 3.2, used a modified thruster to obtain a photographic survey of the discharge evolution. It was found that the discharge does indeed evolve as expected – a concentric collapse culminating in a pinch at the center of the anode.

The design is compact and simple, with no moving parts. A cylinder has the greatest volume per unit base surface area; therefore, the Z-pinch propellant bar, a hollow cylinder, provides the greatest volume of propellant for a given "footprint" size on a spacecraft. The absence of moving parts and compactness may make the AZPPT a good candidate for miniaturization.

Beam divergence is considered to be one of the most negative characteristics of ablative PPTs. The ablation products include carbon "soot" and free fluorine. These compounds may have detrimental effects on other spacecraft systems, such as solar panels. The pinch mechanism in the AZZPT may focus the beam better than conventional rectangular-geometry thrusters.

The principal motivation for developing the AZPPT was to create a thruster with a higher thrust-to-power ratio than its rectangular-geometry counterparts. Our approach to increasing the thrust-to-power ratio is to increase the amount of propellant surface area exposed to the arc. However, doing this may drastically decrease the thrust efficiency because increasing propellant surface area may substantially decrease the propellant utilization efficiency. Mass (or propellant) utilization efficiency in ablative PPTs is low ($< 50\%$) because of two performance robbing processes – late-time vaporization and macroparticle ejection. Both of these phenomena result from the disparate timescales between the current sheet acceleration phase and cooling phase of the propellant surface; the propellant cools on a much longer timescale and, as a result, continues to eject low speed propellant long after the discharge event is over. This wasted propellant is in the form of PTFE vapor and large chunks ($\sim 100\mu$m diameter) of PTFE called macroparticles. Spanjers *et al.* have shown that macroparticles may account for over 30% of the total mass ablated during each pulse[12]. The AZPPT was designed to act as a macroparticle trap. In a rectangular-geometry thruster, macroparticles that leave the surface of the propellant are free to leave the thruster, thus constituting almost a complete loss. The AZZPT provides a geometric prescription to ameliorate this loss mechanism by substantially reducing the free-flight solid angle available for the macroparticles to leave the thruster body. Rather than being lost to space, these particles will be confined to the thrust chamber, eventually coming to rest on the propellant surface or electrodes; hence, these particles will be available propellant in subsequent discharge events.

In the present study, it was postulated that if the macroparticle loss mechanism can be reduced, the amount of exposed propellant surface area can be increased without drastically affecting the overall efficiency. It has been observed that the thrust-to-power ratio scales with the ratio of propellant surface area to total discharge energy[1]. Thus, by controlling the macroparticle ejection, it was hoped that high thrust-to-power ratios could be attained in the AZPPT without sacrificing overall efficiency.

It must be emphasized that the discussion above relates only to our motivation for pursuing the AZPPT development; the physics realized in the actual thrusters may be very different from what we had envisioned. Our purpose in this paper is to demonstrate the performance of the AZPPT; later studies may focus on each of the issues raised above.

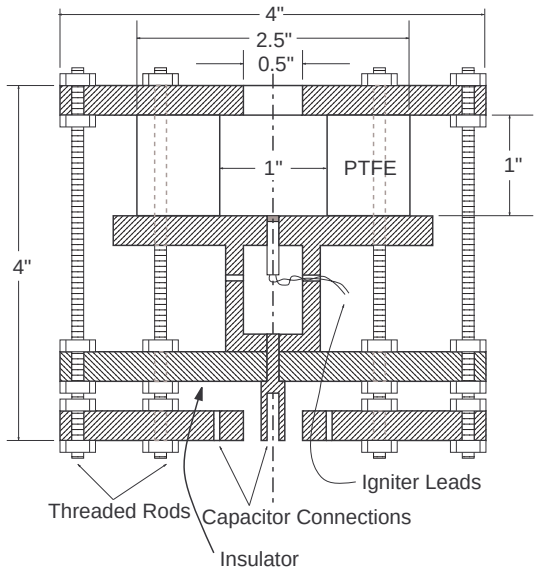

Figure 3: Schematic of AZPPT1.

2.1.2 Design Iterations

In this section we describe in detail the evolution of the AZPPT design. Three generations of the thruster have been tested; knowledge acquired at each stage of the development was implemented in subsequent versions of the thrusters. Performance measurements were used to direct improvements; relevant performance measurements which influenced design changes will be described in general; detailed experimental results for each version are given in section 3.

AZPPT1

The first version of the AZPPT was constructed in 1997 by T. Markusic while working as an intern at AFRL's Electric Propulsion Laboratory. The motivation for building this device was simply to see if an ablative PPT with Z-pinch geometry would work, that is, ignite, ablate PTFE from the insulating sidewalls, and produce thrust. To this end, the accelerator shown schematically in figure 3 was constructed and tested. The thruster used aluminum electrodes, a hollow PTFE cylinder , a polycarbonate insulator/structural member and a Maxwell 33 μF capacitor.

The thruster was operated in AFRL's vacuum facilities and one set of performance data was acquired. The thruster was found to fire repeatably; however, initial performance data was unimpressive (see section 3.1).

AZPPT2

It was apparent that the AZPPT1 geometry has a few shortcomings. Most conspicuously, the amount of parasitic inductance in the structure is unacceptable. Pulsed plasma thrusters must have the smallest possible parasitic inductance in order to get the largest current rise rate (dI/dt) to make conditions favorable for breakdown to occur at the propellant face (i.e. the largest discharge chamber radius.) This implies that the thruster structure should be built to internally contain all of the magnetic flux associated with the discharge current. In AZPPT1 it is clear that the magnetic flux lines that encircle the current-carrying threaded rods are free to bloom out into space; therefore, the AZPPT1 has a high inductance structure. Also, the inter-electrode spacing of AZPPT1 may not be large enough for the thruster to be an effective macroparticle trapper. The particle trapping capability of the discharge chamber is, at least conceptually, more effective as the aspect ratio (AR=height/width) of the chamber is increased. AZPPT1's electrode spacing (which results in AR=0.4-1) was chosen to assure that breakdown would occur; more specifically, the spacing was chosen to be the same as that found in rectangular thrusters that were known to have good breakdown characteristics. This spacing, however, still may not be large enough to effectively trap macroparticles.

A new thruster, AZPPT2, was constructed to remedy the problems associated with the AZPPT1 design. Also, AZPPT2 was used as a testbed for experimenting with new electrode geometries. The basic AZPPT2 thruster, along with two electrode variations, is shown in figure 4.

The parasitic inductance was minimized in AZPPT2 by using completely concentric electrodes with tight tolerances; no magnetic flux is expected to exist outside the thruster body during operation. To increase the discharge chamber aspect ratio, the

height of the discharge chamber was increased by fifty percent to 1.5 inches.

Several other features of AZPPT2 are different than AZPPT1. These changes include new materials, a different igniter arrangement, and a current monitoring device.

Severe erosion of the aluminum electrodes in AZPPT1 was observed. The electrodes in AZPPT2 are made of brass; from visual inspection of the used brass electrodes, it appears that brass is much less susceptible to erosion.

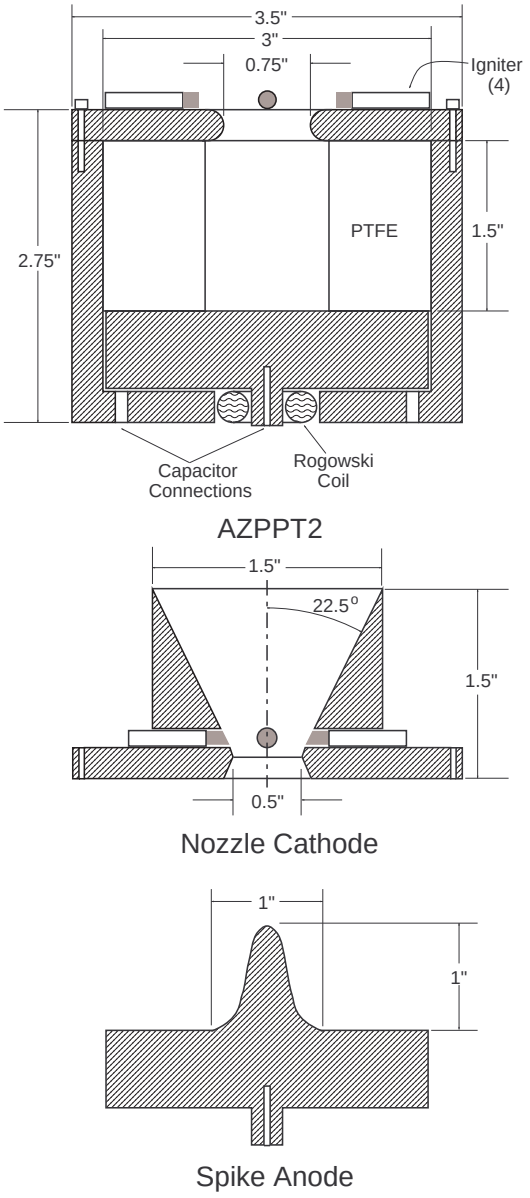

Figure 4: Schematic of basic AZPPT2, nozzle cathode, and spike anode.

Ignition of AZPPT2 was found to be much more repeatable when the igniter was positioned near the cathode. Since, as described in section 2.1, it is preferable to maintain the inner electrode as the anode, the single internal igniter assembly in AZPPT1 was replaced with a radial array of four external igniters in AZPPT2.

A calibrated Rogowski coil was constructed and integrated into the internal structure of AZPPT2. The coil was used to record the current waveform in the thruster during firing. The waveforms were later used to correlate the timing of photographs with current and to better understand the influence of geometric variations on the electrical behavior of the thruster.

Two new types of electrodes were constructed for AZPPT2 – the motivation for which will be described below.

It has been proposed that a large component of thrust in ablative PPTs is derived from electrothermal processes[13]. A large area ratio nozzle, which also served as the thruster cathode, was constructed for AZPPT2 to test whether or not any of the thermal energy in the exhaust could be recovered to produce thrust. A schematic illustration of this nozzle is shown if figure 4. The nozzle has an exit-to-throat area ratio of approximately 10. Four igniters are symmetrically embedded in the nozzle wall near the throat.

A novel “spike” anode was constructed to test some qualitative ideas about how the overall performance of Z-pinch thrusters might be increased. The spike anode was envisioned as a possible way to aid in the turning (conversion of radial compression of the plasma into axial streaming motion) of the flow as well as a geometric prescription to reduce late-time ablation.

The first motivation, flow turning, for using the spike anode stems from the idea of exploiting the tendency of the current sheet to run faster along the anode. If the anode arc attachment of the current sheet moves substantially faster than the cathode attach-

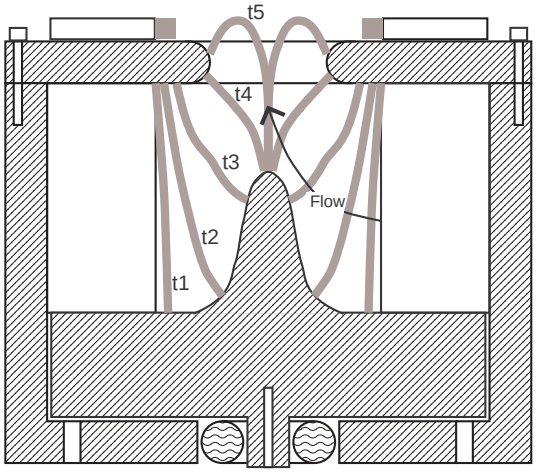

Figure 5: Hypothetical trajectory of current sheet in AZPPT2 with a spike anode for times t1<t2<t3<t4<t5.

ment, the evolution of the discharge might be envisioned to unfold as illustrated in figure 5. If the actual discharge were to progress as illustrated in this hypothetical example, one would expect that the plasma would arrive at the pinching region (tip of the anode) with considerable axial speed, thus relaxing the need to convert pure radial motion into axial motion along a thin current filament. In short, the spike anode conceptually shows a way to improve the specific impulse of a Z-pinch thruster.

The second motivation for using a spike anode concerns the possible reduction of late time-ablation. After discharge initiation the current sheet accelerates away from the propellant face; however, the current sheet continues to transfer energy to the propellant surface via radiation and thermal conduction. The ideal way to reduce late-time ablation would be to allow the current sheet to pick up its initial load of propellant, then immediately optically and thermally isolate it from the propellant. Since this ideal situation is not achievable, a practical design would strive to get the arc out of the discharge chamber as quickly as possible. The spike anode may partially achieve this scenario by guiding part of the current lines into a blowing mode outside of the thrust chamber as illustrated in figure 5.

For the reasons described above, a spike anode was constructed and tested with AZPPT2. An immediate question is what shape and height the spike should have. In the first iteration of the spike concept a fairly blunt and short spike was chosen out of fear that the discharge might choose to initiate at the tip of the spike rather than along the surface of the PTFE. In the end, the spike concept proved to significantly enhance the thruster performance. The details of performance for all configurations of AZPPT2 are given in section 3.2.

In order to better understand the current sheet dynamics of the ablative Z-pinch thrusters, a modified version of AZPPT2 was constructed. This thruster used a mesh sidewall and clear acrylic propellant to allow visual access to the discharge chamber. Photographs of the thruster firing, taken using a high speed framing camera, are presented in section 3.2.

AZPPT3

The next major design iteration resulted in AZPPT3. The changes in the overall design from AZPPT2 to AZPPT3 were far less severe than the those that occurred in going from AZPPT1 to AZPPT2. As will be shown in section 3.2, AZPPT2 had substantially higher performance than AZPPT1. Further, it was found that the most promising geometry was the combination of spike anode and orifice cathode. While the specific impulse of AZPPT2 with the spike anode and orifice cathode was found to be higher than any other configuration, the thrust-to-power ratio and efficiency were lower. The motivation for building AZPPT3 was to increase the thrust-to-power ratio and efficiency while maintaining the higher specific impulse. It was thought, continuing with rational that led to AZPPT2, that is, increasing of the discharge chamber aspect ratio, would give the desired result. To this end, the discharge chamber height was increased by fifty percent. Also, the outer radius of the propellant was reduced so that AZPPT3 contained the same amount of propellant as AZPPT2.

In AZPPT3 the spike anode was made to be (proportionally) taller than in AZPPT2. It was hoped that the taller, thinner anode would even further exploit the spike anode design principals – flow turning and

arc ejection.

Further, more superficial improvements to AZPPT3 included a more easily serviceable structure and a removable igniter module. A schematic and photograph of AZPPT3 are shown in figure 6.

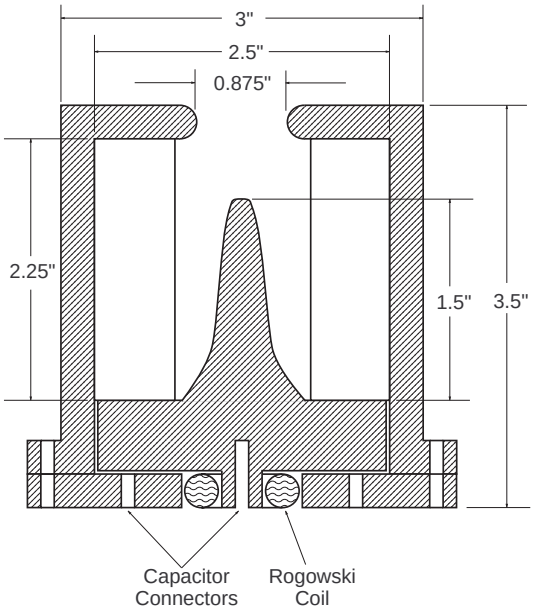

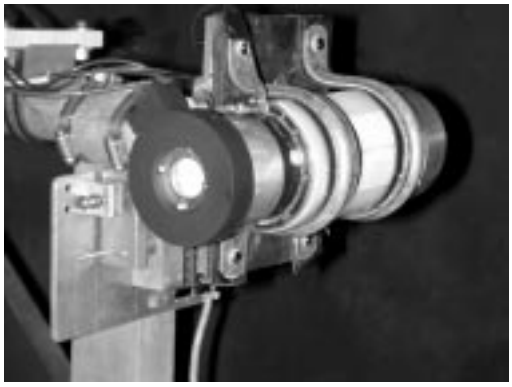

Figure 6: Schematic and photograph of AZPPT3 on thrust stand.

3 Experimental Results

In this section the details of the experimental procedure and performance data will be presented for each of the designs discussed in the previous section. The motivation for the design changes discussed earlier will be described in more detail with the support of experimental data.

3.1 AZPPT1

The most significant result of the testing of the AZPPT1 thruster was the proof-of-concept, that is, that the thruster fired repeatably and ablated PTFE to produce thrust. The thruster was fired with 40 J capacitor energy at 1 Hz pulse frequency for over 50,000 total shots. Only one performance measurement was carried out on the AZPPT1 geometry. Impulse measurements were obtained using AFRL's pulsed plasma thruster thrust stand. The impulse bit was found to be approximately 600 μN-s. Using the measured value of m_{bit}, approximately 250 μg/shot, the calculated values for the performance parameters are: $I_{sp} \sim 240$ s, $\eta_t \sim 2\%$, and $T/P \sim 15$ μN/W. As only a single data point was taken, the results are not statistically meaningful; nevertheless, the measurement serves as a rough benchmark to evaluate the effectiveness of the subsequent design iterations.

3.2 AZPPT2

Performance measurements were carried out on AZPPT2 for four different electrode configurations. Also, two different propellant radii were used for each electrode combination. Table 1 summarizes all of the AZPPT2 configurations tested.

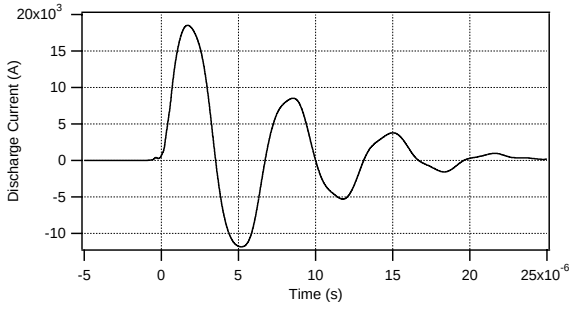

Figure 7: Typical discharge current trace in AZPPT2 for trial number 1.

Trial	Anode	Cathode	Propellant ID [in]
1	F	O	1
2	F	O	1.5
3	F	N	1
4	F	N	1.5
5	S	O	1
6	S	O	1.5
7	S	N	1

Table 1: Summary of AZPPT2 configurations. F=Flat Anode, S=Spiked Anode, O=Orifice Cathode, N=Nozzle Cathode. The corresponding data is found in figure 8

In all configurations a 38.3 μF Maxwell capacitor was used; the stored capacitor energy for all trials was 76 J (2 kV capacitor voltage). This corresponded to the maximum voltage rating of the capacitor. The discharge current waveform for all of the configurations are very similar; a typical current waveform, measured using the integrated Rogowski coil, from trial number one is shown in figure 7. The thruster current exhibits damped sinusoidal behavior typical of ablative pulsed plasma thrusters.

The results for all data runs are summarized in figure 8. The measured impulse bit, mass bit and calculated values for specific impulse, thrust efficiency, and thrust-to-power ratio for each trial are plotted.

Several conclusions can be inferred from the data. First, it is evident that AZPPT2 significantly outperformed AZPPT1 in all respects. In particular, the specific impulse increased by up to 100%, the thrust efficiency increased by up to 400%, and the thrust-to-power-ratio increased by up to 300%.

All AZPPT2 configurations showed a moderate decrease in all performance parameters with the larger inner diameter propellant cylinder. However, marked differences in performance were found with different electrode arrangements. The nozzle cathode performed worse than the simple orifice cathode for all performance parameters. The combination of flat anode and orifice cathode showed the highest thrust efficiency and thrust-to-power ratio. The combination of spike anode and orifice cathode showed the highest specific impulse, but lower thrust efficiency and thrust-to-power ratio.

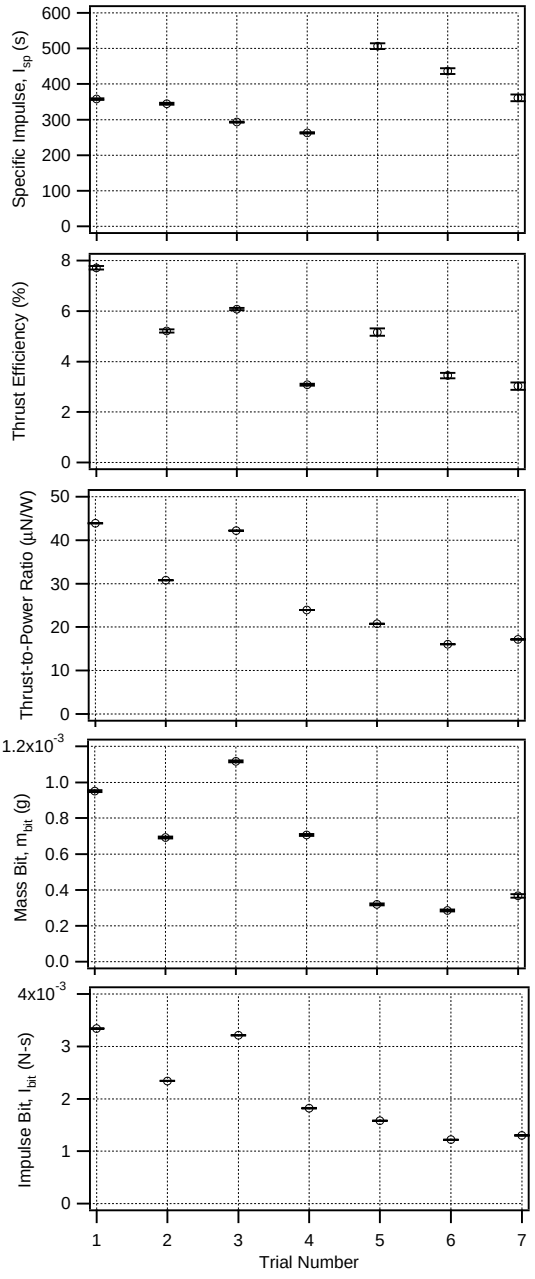

Figure 8: AZPPT2 data summary at 76 J.

Photographs of the evolution of the discharge were

taken using an Imacon 760LC fast framing camera. The modified AZPPT2 thruster with transparent Plexiglas propellant, mesh sidewalls, and spike anode was arranged so that a side-view of the discharge could be photographed. The framing rate was set to 500 kHz; up to eight pictures could be obtained in a single run. A 590 nm interference filter, which corresponds to a strong carbon ion line[14], was used. Figure 9 shows a sequence of photographs during a single discharge event while figure 10 shows the discharge fully pinched at the tip of the spike anode. The photographs show that, as expected, the discharge initiates near the propellant face, climbs the anode, and finally pinches at the tip of the anode.

Figure 9: Sequence of high speed photographs of the discharge inside AZPPT2 with transparent Plexiglas propellant and mesh sidewalls (thruster sketched in for clarity. Dark object protruding down into the plasma is a structural member in the Plexiglas). Photos obtained using a 590 nm filter. The dashed line highlights the evolution of the current sheet.

3.3 AZPPT3

More detailed performance measurements were carried out on AZPPT3 than on any individual configuration of AZPPT2. In particular, data was acquired with two different capacitors, two different propellant radii, and several different energy levels. Two Maxwell capacitors supplied by the Primex Corp. were used: 33.6 and 38.3 μF. Propellant diameters of 1 and 1.5 inches were tested. Four stored capacitor energies were used: 25, 50, 67, and 75 J.

Figure 11 shows a collection of impulse bit measurements for the 38.3 μF capacitor. It is seen that the impulse bit remains relatively constant after 100 shots. The initial decay in impulse bit is most likely due to surface contamination of the propellant from adsorbed gas or vacuum pump oil.

Figures 12 and 13 show the calculated performance parameters for all measurements made. Reflecting on the motivation for building AZPPT3 as described in section 2.1.1, the data shows that the goals have been realized – higher thrust-to-power ratio and efficiency while maintaining a high specific impulse. In fact, the specific impulse actually increased with this configuration. Comparing the data for AZPPT3 with the data in figure 8 for AZPPT2 at 76 J shows that specific impulse increased at that energy level on the order of 10%, thrust efficiency by roughly 15%, and thrust-to-power ratio by 30%.

Other trends are evident in the graphs. The top graph of figure 12 shows that, in general, specific impulse increases with propellant radius for a given energy: however, the lower two graphs show that

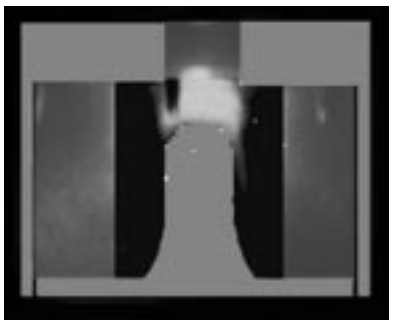

Figure 10: High speed photograph showing the discharge fully pinched inside AZPPT2 with transparent Plexiglas propellant and mesh sidewalls (thruster sketched in for clarity. Dark object protruding down into the plasma is a structural member in the Plexiglas). Photos obtained using a 590 nm filter.

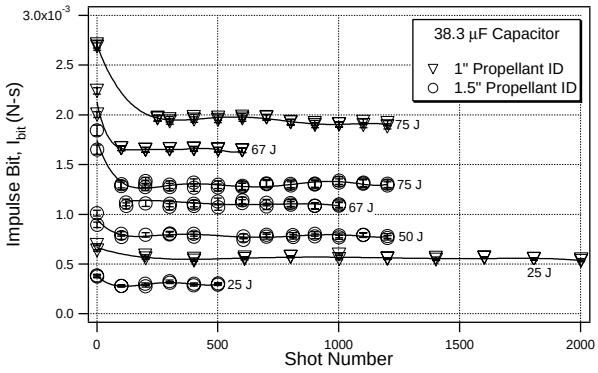

Figure 11: Impulse bit as a function of the number of shots fired for AZPPT3 using a 38.3 μF capacitor. Multiple energies shown.

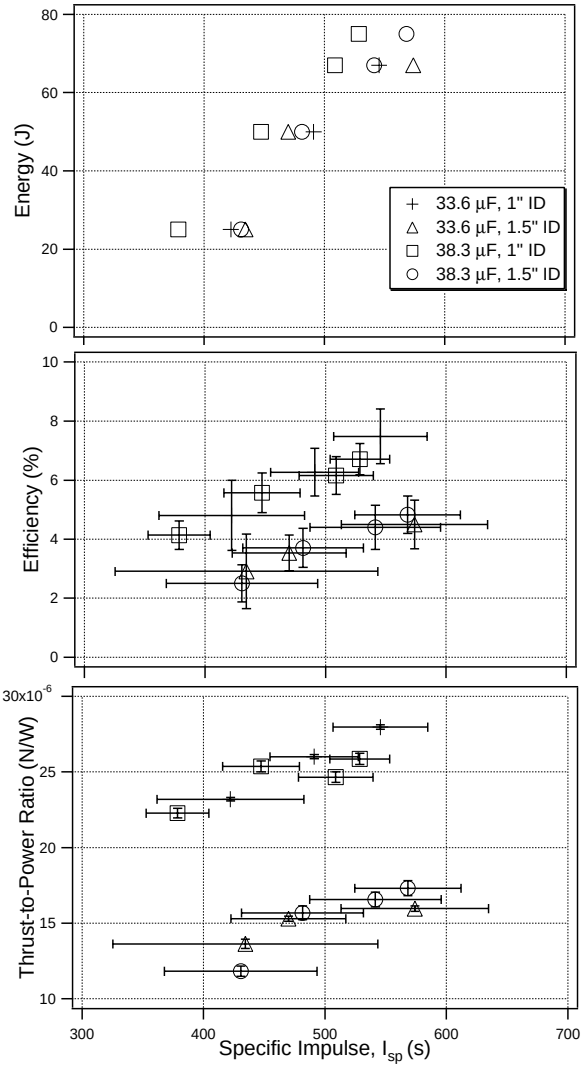

Figure 12: AZPPT3 performance parameters as a function of I_{sp}.

both efficiency and thrust-to-power ratio decrease with propellant radius. Also, all three graphs show that all performance parameters are higher for the smaller capacitance; peak performance parameters for the 33.6 μF capacitor are: $I_{sp} = 574$ seconds, efficiency = 7.5 %, and thrust-to-power ratio = 28 μN/W. In general, all performance parameters increase with impulse bit and specific impulse.

There are three potential sources of error in the present work: error associated with the measurement of the impulse bit, error associated with the measurement of the mass bit, and lack of information about the electrode erosion rates. Of the two quantified errors, the error on the measurement of the mass bit is much larger than that associated with the measurement of the impulse bit. The mass bit error is the main source of error in the calculated performance parameters. As the thruster fires, the propellant bar experiences a transient where its temperature rises and the mass bit increases[3]. Since the experiments undertaken were all relatively short in duration (≤ 2000 shots) it was possible that the thruster was still operating in this transient regime and the mass bit measured was not the steady-state value. To

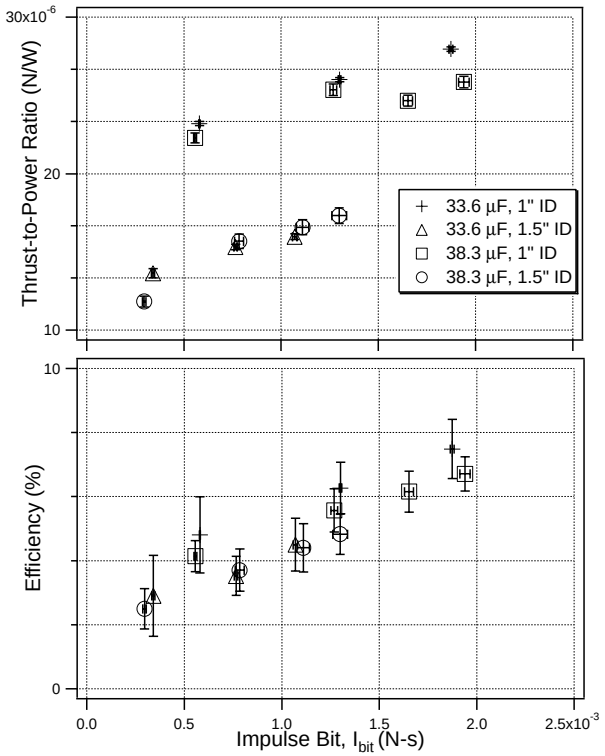

Figure 13: AZPPT3 performance parameters as a function of impulse bit.

test this, a longer duration (4000 shot) experiment was run at the 25 J energy level. The mass bit from the 4000 shot experiment matched the corresponding 2000 shot mass bit within the error bars, so it was concluded that the transient propellant temperature effects did not contribute to the error on the mass bit. Since no attempt was made to measure electrode erosion rates, its impact on the thruster performance is uncertain.

4 Conclusions

A series of ablative pulsed plasma thrusters have been constructed and tested; the motivation for the study was to develop a thruster with a high thrust-to-power ratio and reasonable efficiency. The approach pursued for increasing the thrust-to-power ratio was to construct a thruster with a large exposed propellant area. In order to avoid the potential negative impact of a large exposed propellant area on efficiency (that is, very low mass utilization efficiency associated with late time ablation), the Z-pinch geometry was chosen to exploit its potential macroparticle trapping capabilities.

An iterative design process culminated in a novel Z-pinch thruster with a spike anode. The peak performance parameters of this thruster, designated AZPPT3, were found to be: $I_{sp} = 574$ seconds, efficiency = 7.5 %, and thrust-to-power ratio = 28 μN/W. Also, a photographic survey obtained using a modified thruster gave insight into the current sheet dynamics and showed the plasma Z-pinch effect taking place.

Conclusions reached in this study were:

- Flow turning can be realized in the ablative Z-pinch thruster geometry to obtain thrust.
- The dynamics of the current sheet in an ablative Z-pinch thruster are similar to those found in a gas-fed Z-pinch thruster.
- Losses associated with the use of a nozzle outweigh any benefits from the recovery of the plamsa's thermal energy.
- Increasing the aspect ratio of the discharge chamber increases the thrust-to-power ratio.
- In high aspect ratio configurations, the efficiency and specific impulse can be maintained through the use of a spike anode.

Several potential benefits of the Z-pinch geometry were described in section 2.1.1. Since this study only addressed global performance, future work should include experiments to address each of these points directly. Also, the extent to which the aspect ratio of the discharge chamber can be increased for benefit should be explored. Current waveform tailoring, for example through the use of diodes, may also prove worthwhile to pursue.

Acknowledgements

The authors gratefully acknowledge Primex Corp. for supplying the capacitors used during this project, and Robert Sorenson for his technical contributions.

References

[1] P.J. Turchi and R.L. Burton. Pulsed plasma thruster. *J. Propulsion and Power*, 14(5):716–735, Sept.-Oct. 1998.

[2] M. Martinez-Sanchez and J.E. Pollard. Spacecraft electric propulsion - an overview. *J. Propulsion and Power*, 14(5):688–699, Sept.-Oct. 1998.

[3] G. Spanjers. Propellant inenefficiencies in pulsed plasma thrusters. In 6^{th} *Aerospace Sciences Meeting*, New York, New York, January 22-24 1968. AIAA 68-85.

[4] W.J. Guman. Solid propellant pulsed plasma micro-thruster studies. In 6^{th} *Aerospace Sciences Meeting*, New York, New York, January 22-24 1968. AIAA 68-85.

[5] R.J. Vondra, K.I. Thomassen, and A. Solbes. Analysis of solid teflon pulsed plasma thruster. *Journal of Spacecraft and Rockets*, 7(12):1402–1406, December 1970.

[6] W.L. Ebert, S.J. Kowal, and R.F. Sloan. Operational Nova spacecraft teflon pulsed plasma thruster system. In 25^{th} *Joint Propulsion Conference*, Monterey, California, July 10-12 1989. AIAA 89-2497.

[7] E. Antonsen, R.L. Burton, and F. Rysanek. Energy measurements in a coaxial electromagnetic pulsed plasma thruster. In 35^{th} *Joint Propulsion Conference*, Los Angeles, CA, June 20-24 1999. AIAA 99-2292.

[8] I.G. Mikellides and P.J. Turchi. Optimization of pulsed plasma thrusters in rectangular and coaxial geometries. In 26^{th} *International Electric Propulsion Conference*, Kitakyushu, Japan, October 17-21 1999. IEPC 99-211.

[9] T.E. Markusic and E.Y. Choueiri. Visualization of current sheet canting in a pulsed plasma accelerator. In 26^{th} *International Electric Propulsion Conference*, Kitakyushu, Japan, October 17-21 1999. IEPC 99-206.

[10] C.D. Challis, P. Choi, A.E. Dangor, and M.G. Haines. Time and space resolved x-ray measurements on a gas-puff z-pinch. In *Proc. 12th Eur. Conf. Contr. Fusion Plasma Phys.*, pages 72–75, 1985.

[11] R.G. Jahn, W. Jaskowsky, and R.L. Burton. Ejection of a pinched plasma from an axial orifice. *AIAA Journal*, 3(10):1862–1866, October 1965.

[12] G.G. Spanjers, J.S. Lotspeich, K.A. McFall, and R.A. Spores. Propellant losses because of particulate emission in a pulsed plasma thruster. *J. Propulsion and Power*, 14(4):554–559, July-Aug. 1998.

[13] D.R. Keefer and B. Rhodes. Electromagnetic acceleration in pulsed plasma thrusters. In 25^{th} *International Electric Propulsion Conference*, Cleveland, OH, August 1997. IEPC 97-035.

[14] T.E. Markusic and R.A. Spores. Spectroscopic emission measurements of a pulsed plasma thruster. In 33^{rd} *Joint Propulsion Conference*, Seattle, WA, July 6-9 1997. AIAA 97-2924.

[15] A.C. Ducati, R.G. Jahn, E. Muehlberger, and R.P. Treat. Exploratory electromagnetic thruster research. Annual Report NASA Report CR62047, Giannini Scientific Corporation, February 1968.

[16] E.A. Cubbin, J.K. Ziemer, E.Y. Choueiri, and R.G. Jahn. Pulsed thrust measurements using laser interferometry. *Review of Scientific Instruments*, 68(6):2339–2346, June 1997.

[17] J.K. Ziemer, E.Y. Choueiri, and D. Birx. Is the gas-fed ppt an electromagnetic accelerator? An investigation using measured performance. In 35^{th} *Joint Propulsion Conference*, Los Angeles, California, June 20-24 1999. AIAA 99-2289.

A Test Facility

This appendix serves to introduce a major new testing facility to the electric propulsion community and documents the measures taken to quantify and control the amount of contamination due to residual gases. Such measures are crucial for legitimate performance claims when dealing with low impulse devices such as PPTs.

A.1 Vacuum Chamber

Recently at EPPDyL, a new, large dielectric vacuum facility has been brought on-line. This chamber was originally constructed in 1965 for electromagnetic propulsion research at the Giannini Scientific Corporation. In 1975, the chamber was donated to EPPDyL where it remained, unused, until it was refurbished in 1998.

The vessel is approximately 25 feet in length with an inner diameter of 8 feet in the test section and possesses an internal volume of approximately 27,000 liters (see fig. 14).

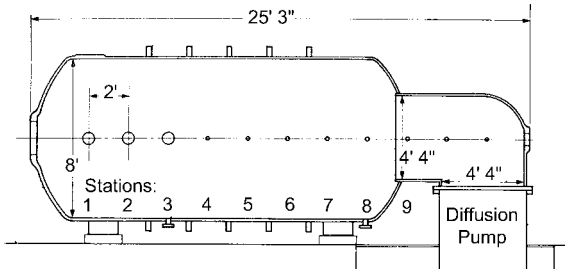

Figure 14: Schematic of the EPPDyL new large dielectric facility (modified from ref. [15]).

The facility was constructed through a process of spraying fiberglass one layer at a time until the desired thickness was reached. A black polyester gel coat containing carbon black forms the innermost layer (for details, see [15]). The choice of a dielectric like fiberglass was made for two reasons. The first was to eliminate the possibility of induced currents in the tank structure that might affect the measurement of an electric thruster's performance. The second was to allow for the possibility of setting up

Figure 15: Large dielectric facility.

equipment, such as antennas, outside the chamber for making thruster interference measurements. The inner surface was made black to give a good background for photography, and the material type was chosen for its reduced outgassing properties. Optical access throughout the chamber is provided by 31 windows..

A.2 Pumping System

The chamber is equiped with a 95,000 L/sec, 48" high-vacuum diffusion pump with a 3000 cfm roughing pump system consisting of a Roots Blower and two Stokes mechanical pumps backing it. Although both Stokes pumps can be operated simultaneously, a good vacuum of 1×10^{-5} torr or less is attainable with only one in operation.

A.3 Liquid Nitrogen Cold Trap

In an effort to reduce backstreaming of oil from the diffusion pump, a liquid nitrogen baffle system was designed and implemented. These baffles (see fig. 16) have been designed to present an optically thick view of the main test chamber to the diffusion pump, while at the same time being as optically thin as possible to any propellants or other gases flowing out of the test chamber. The spacing between the baffle plates is 6 inches, which is on the order of the mean

free path of a particle of diffusion pump oil at around 5×10^{-5} torr, and the overlap between plates helps to ensure that oil particles will have at least one collision with the cold trap before entering the tank.

Figure 16: Liquid Nitrogen cold trap

Station	Without Baffles	With Baffles	% Reduction
1	1.4	0.6	57 %
2	4.9	0.8	84 %
3	4.9	0.9	82 %
4	5.1	1.0	80 %
5	5.8	0.9	84 %
6	3.0	0.7	77 %
7	9.3	1.9	80 %
8	12.0	1.7	86 %
9	20.9	5.6	73 %

Table 2: Vacuum pump oil backstreaming rates with and without the baffles installed (in $[\mu\mathrm{g\ m^{-2}\ s^{-1}}]$).

Two tests were performed to evaluate the performance of the cold trap. The first was aimed at quantifying the effectiveness of the design, while the second was performed to determine quantitatively the exit temperature to which the trap coolant should be regulated. The results of the first test are seen in table 2. These were obtained by placing clean plates at stations throughout the chamber, running the vacuum system for over six hours, and then weighing the plates to determine the level of oil backstreaming. The stations along the chamber are labeled in figure 14. As can be seen, this design significantly reduces the amount of backstreaming into the test chamber.

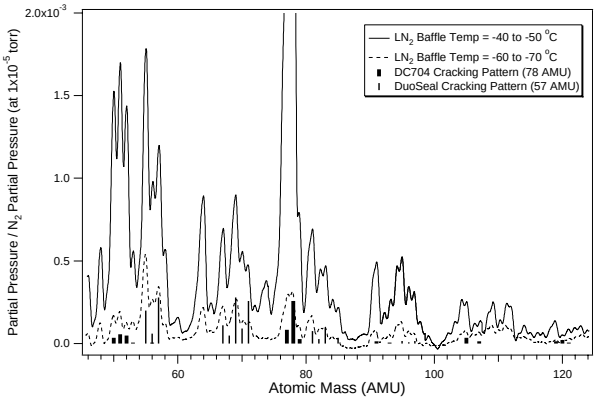

Figure 17: Background gas mass spectrum at different baffle outlet temperatures and the expected cracking patterns of DuoSeal roughing pump oil and DC704 diffusion pump oil

Thrusters studied in this paper were pulsed at a frequency of 0.5 Hz. The thrust stand is located at station 2 and, in the worst case, the area of the orifice propellant is ejected from is $\sim 2.9 \times 10^{-4}$ m^2. From the pulse frequency, orifice area, and data in table 2, the flux of oil into the thruster is $\sim 4.6 \times 10^{-4}$ μg per shot. The smallest mass bit measured was roughly five orders of magnitude greater than this deposition rate. Therefore, the contamination error introduced into the mass bit measurement due to oil deposition on the propellant face can be neglected.

The second experiment was performed using a UTI 100C residual gas analyzer (RGA) to measure the level of oil vapor in the background gas. This test was used to determine the temperature at which the cold trap outlet temperature should be regulated. Regulation is accomplished by means of a liquid nitrogen valve and active control system which samples the baffle cooling line outlet temperature. A mass spectrum of partial pressures is shown in figure 17 for the mass range where diffusion and rough-

ing pump oil is prevalent. The partial pressures are normalized by the partial pressure of nitrogen gas measured at 1×10^{-5} torr. The N_2 background gas partial pressure turns out to be about 5×10^{-6} torr. Data were acquired for colder exit temperatures, but there are diminishing returns below the -60 to $-70°C$ case, so those plots have been omitted from figure 17 for clarity. Reductions in the residual gas background contribution due to diffusion and roughing pump oil for the two different exit temperatures shown is seen typically to be greater than 70%.

A.4 Thrust Stand

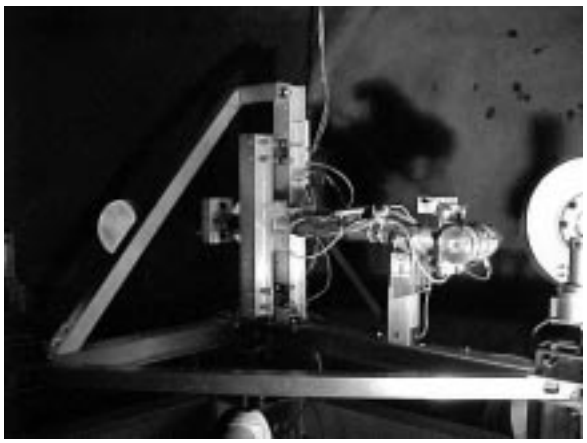

Figure 18: Thrust stand

A swinging-gate style microbalance thrust stand capable of measuring extremely small impulse bits was recently designed and implemented. It is the latest design iteration in a series of micro-thrust stands which include an earlier one at EPPDyL [16] and one at NASA-JPL [17].

A Linear Voltage Displacement Transducer (LVDT) is used to measure and record the motion of the arm. The dynamics of this motion can then be analyzed as a simple spring-mass-damper system to determine the performance of the thruster being tested. Variables in the spring-mass-damper system can be determined through a pre-experiment calibration. A full discussion of thrust stand dynamics can be found in [16].

The primary feature of the new thrust stand is its active damper circuit. A solenoid has current driven through it, inducing a magnetic field which drives a ferromagnetic rod mounted to the thrust stand arm. The solenoid signal is proportional to the time derivative of the arm position, thus maintaining this as a simple spring-mass-damper system. Since the arm should be relatively still before pulsing the thruster, this active damping system allows for a minimization of the time between thruster firings.